J. Geophys. 48, 181–194, 1980

Journal of Geophysics

Geomagnetic Induction Studies in Scandinavia

I. Determination of the Inductive Response Function from the Magnetometer Array Data

A.G. Jones
Institut für Geophysik, Gievenbecker Weg 61, D-4400 Münster, Federal Republic of Germany

Abstract. Data from the Münster IMS Magnetometer Array (Küppers et al. 1979) have been analysed in the frequency domain to derive the inductive response function, $C(\omega, 0)$, from the ratio of the vertical magnetic field to the spatial gradient of the horizontal magnetic field. The response function was best determined by statistical frequency analysis techniques after the spatial gradients had been derived by least-squares fitting of two-dimensional second-order polynomials to the observations, with the constraint imposed that the solutions be curl-free.

The derived response function was found to obey two different causality requirements, and most of the inequality constraints imposed on it (Weidelt 1972). A preliminary model, in which conductivity is a function of depth only and which explains the major details of the observed response, is presented. It has a highly resistive uppermost layer of some 10^4 Ωm and of the order of 30 km thick, underlain by a layer of about 125 Ωm to a depth of around 140 km, where a transition takes place to a highly conducting (3 Ωm) half space.

The effect of various non-uniform sources on the observations of $C(\omega, k)$ for this 1D model is illustrated.

Key words: Magnetometer arrays – Response function analysis – Geomagnetic induction studies in Scandinavia.

1. Introduction

This is the first in a series of papers treating various aspects of geomagnetic induction in Scandinavia as observed by the Münster IMS Magnetometer Array (Küppers et al. 1979) and by concurrent telluric field recording at some locations. This paper will deal principally with the inductive response function, $C(\omega, k)$, its properties, its determination and its validity, from magnetometer array data. Other papers will be concerned with the more traditional geomagnetic depth sounding (GDS) and magneto-telluric (MT) techniques, modelling studies, and a geophysical interpretation of all the results obtained.

Geomagnetic induction studies using large arrays of magnetometers began with the introduction of a cheap but very fieldworthy instrument by Gough and Reitzel (1967). Since that time, many array studies have been made in various countries (see the map of world activity in Lilley 1975) and reviews by Porath and Dziewonski (1971), Gough (1973a, b), Frazer (1974) and Lilley (1975) summarise the usual methods employed to analyse and present the data. These comprise *qualitative* analysis methods; e.g., mapping Fourier terms, induction vectors, inspection of magnetograms; *quantitative* analysis methods; e.g., separation of internal and external parts, determination of horizontal layering from Z/H ratios, determination of horizontal layering employing the ratio of the vertical field to the spatial gradient of the horizontal field; and *modelling* techniques, from primitive depth-of-line-current determinations to general 2D or 3D numerical or analytical techniques.

Of all these, the method involving the determination of the ratio of the vertical magnetic field to the horizontal spatial gradient, hereafter referred to as the HSG (horizontal spatial gradient) method, has attracted the least interest. Since the relationship between this ratio and the magnetotelluric impedance was shown by Schmucker (1970), Kuckes (1973a, b), and in a global sense by Berdichevsky et al. (1976), this HSG method has only been appied to magnetometer array data by Kuckes (1973a), Lilley and Sloane (1976) and Woods and Lilley (1979). The first two studies cited above derived the spatial gradients from published maps of the Fourier horizontal field components, which did not permit any determination of the coherence between the vertical field and the horizontal spatial gradient field. Woods and Lilley fitted fields at Fourier harmonics to three complex two-dimensional surfaces, one for each component, but restricted themselves to quiet daily variations and the first four harmonics thereof.

In this work, the spatial gradients are determined by least-squares fitting of 2D second-order surfaces to the observed fields, with the curl-free constraint imposed on the solutions, and the inductive response function is derived by statistical frequency analysis methods, with corresponding coherences and confidence interval estimations. The response function can be determined down to short periods (100 s) due to the large gradients observed at these periods in the auroral zone. The derived function is tested for physical realisability, i.e., causality and validity, and a preliminary one-dimensional model that explains the major details is given. The effects of non-uniform source fields, in the form of non-zero values for Price's (1962) wavenumber, and of Gaussian electrojets on the theoretical response function calculated from the 1D model is illustrated.

2. Theory

In this section the inductive response function is defined and its properties stated. For a complete exposition, the reader is referred to Schmucker (1970), Weidelt (1972, 1978), Kuckes (1973a, b) and Lilley (1975).

0340-062X/80/0181/$02.80

2.1. The Inductive Response Function $C(\omega, k)$

Defining the inductive response function, $C(\omega, k)$, for a single wave vector field $\mathbf{k}=(k_x, k_y)$, by the relationship

$$C(\omega,k)=\frac{H_z(\omega)}{\frac{\partial}{\partial x}H_x(\omega)+\frac{\partial}{\partial y}H_y(\omega)}, \tag{1}$$

where $k=(k_x^2+k_y^2)^{\frac{1}{2}}$, the absolute value of the tangential wave number $(k=2\pi/\lambda)$,

and $\mathbf{H}(\omega)=(H_x(\omega), H_y(\omega), H_z(\omega))$, the three orthogonal components of the magnetic field at frequency ω,

it is simple to derive that, *over a* 1D *earth* (i.e., conductivity a function of depth only, $\sigma(z)$), this function is related to the magneto-telluric impedance function $Z_{xy}(\omega, k)$, by

$$C(\omega,k)=\frac{1}{i\omega\mu_0}\cdot Z_{xy}(\omega,k) \tag{2}$$

(Schmucker 1970; Kuckes 1973a, b; Schmucker and Weidelt 1975). This is a direct consequence of the fact that, for a 1D earth, the magneto-telluric impedance tensor, $\mathbf{Z}$, assumes the well-known Cagniard type form, viz.

$$\mathbf{Z}=\begin{bmatrix} 0 & Z_{xy} \\ -Z_{xy} & 0 \end{bmatrix} \tag{3}$$

(Cagniard 1953). Following the notation of Weidelt (1972), the real and imaginary parts of $C(\omega, k)$ shall be denoted by $g(\omega)$ and $-h(\omega)$ respectively, from

$$C(\omega,k)=g(\omega,k)-ih(\omega,k). \tag{4}$$

2.2. General Properties of a Response Function

Consider a simple time-independent linear system as illustrated in Fig. 1. The input, $i(t)$, is related to the output $o(t)$, by the convolution integral

$$o(t)=\int_{-\infty}^{\infty} h(\tau)\, i(t-\tau)\, d\tau$$

where $h(\tau)$ describes the dynamic characteristics of the system, and is commonly termed the impulse response function. The function $h(\tau)$ must display certain characteristics if the system is to be *physically realisable*; it must not respond before receiving any input. This causality condition requires that

$$h(\tau)=0 \quad \tau<0 \tag{5}$$

hence the integral should only be determined in the range $(0, \infty)$, i.e., for all positive lags.

Fourier transformation of the above convolution integral yields

$$O(\omega)=H(\omega)\cdot I(\omega) \tag{6}$$

where $H(\omega)$ is termed the transfer function and is related to $h(\tau)$ by

$$H(\omega)=\int_0^{\infty} h(\tau)\, e^{-j\omega\tau}\, d\tau.$$

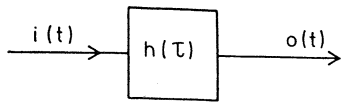

Fig. 1. Single input – single output linear system with the input, $i(t)$, related to the output, $o(t)$, by the dynamic characteristics of the system, $h(\tau)$

As shown by Solodovnikov (1952), (repeated in Kanasewich 1973), the real and imaginary parts of a causal transfer function describing a linear system are *not* independent, but are related by the Hilbert transform, viz.

$$H_R(\omega)=\mathscr{H}\{H_I(\omega)\}=\frac{1}{\pi}P\int_{-\infty}^{\infty}\frac{H_I(w)}{\omega-w}\,dw \tag{7a}$$

$$H_I(\omega)=-\mathscr{H}\{H_R(\omega)\}=-\frac{1}{\pi}P\int_{-\infty}^{\infty}\frac{H_R(w)}{\omega-w}\,dw \tag{7b}$$

where $H_R(\omega)$ and $H_I(\omega)$ are the real and imaginary parts of $H(\omega)$ respectively, and P denotes the Cauchy principal value of the integral. For minimum phase systems, the relationships may be rewritten to show that if $H(\omega)=|H(\omega)|\,e^{i\phi(\omega)}$, then $\log|H(\omega)|$ is related to $\phi(\omega)$ by the Hilbert transform. Relationships (7a) and (7b) are termed the Kramers-Kronig relations in atomic scattering theory and Bode's relations in servo-mechanics.

2.3. Properties of the Inductive Response Function

The inductive response function, $C(\omega, k)$, as defined by (1), possesses certain properties due to the fact that the earth has a finite, positive conductivity, i.e., $0<\sigma<\infty$. Recalling that $C=g-ih$ (dependence on frequency and wavenumber assumed), and defining the operator D to denote

$$Df=\frac{\omega\, df}{d\omega}=\frac{df}{d\log\omega}=-\frac{df}{d\log T},$$

the following inequalities apply (Weidelt 1972, Eqs. 2.30–2.34)

$$g\geqq 0 \quad h\geqq 0, \tag{8a, b}$$

$$Dg\leqq 0, \tag{9}$$

$$0\leqq -D|C|\leqq|C|, \tag{9a, b}$$

$$|DC|\leqq h, \quad |C+DC|\leqq g, \tag{11a, b}$$

$$|D^2C|\leqq h, \quad |C+2DC+D^2C|\leqq g. \tag{12a, b}$$

The limiting values of the terms g and h at high and low frequencies are

$$g=\begin{cases}\dfrac{1}{k}\tanh(kd) & \text{for } \omega\to 0 \qquad (13a)\\[2ex] \dfrac{1}{(2|\omega|\,\mu_0\sigma_1)^{\frac{1}{2}}} & \text{for } \omega\to\pm\infty, \qquad (13b)\end{cases}$$

$$h=\begin{cases}0 & \text{for } \omega\to 0 \qquad (13c)\\[2ex] \dfrac{\pm 1}{(2|\omega|\,\mu_0\sigma_1)^{\frac{1}{2}}} & \text{for } \omega\to\pm\infty \qquad (13d)\end{cases}$$

where k is as given in Eq. (1)
d is the depth of the perfect conductor
σ_1 is the conductivity of the top layer

and μ_0 is the permeability of free space,
and the function C satisfies

$$C(-\omega)=C^*(\omega) \tag{14}$$

such that g is symmetric and h anti-symmetric about the $\omega=0$ axis.

As shown by Weidelt [1972, Eq. (2.19)], the inductive response function admits the representation

$$C(\omega)=\int_0^\infty \frac{a(\lambda)}{\lambda+j\omega}\,d\lambda$$

where $a(\lambda)$ is a generalised function given by

$$a(\lambda)=-\lim_{\varepsilon\to+0}\frac{1}{\pi}\operatorname{Im}(C(j\lambda+\varepsilon))\geqq 0$$

(Schmucker and Weidelt 1975, the non-negativity of which ensures that C must be a smooth function of frequency. Using the result

$$\frac{1}{2\pi}\int_{-\infty}^{\infty}\frac{e^{j\omega t}}{\lambda+j\omega}\,d\omega=\frac{1}{2\pi j}\int_{-\infty}^{\infty}\frac{e^{j\omega t}}{\omega-j\lambda}\,d\omega$$
$$=\begin{cases}0 & t<0\\ e^{-\lambda t} & t>0\end{cases}$$

($\lambda>0$) obtained by closing the contour for $t<0$ in the lower ω-halfplane, and for $t>0$ in the upper, it follows that

$$c(t)=\frac{1}{2\pi}\int_{-\infty}^{\infty}C(\omega)\,e^{j\omega t}\,d\omega$$
$$=\begin{cases}0 & t<0\\ \int_0^\infty a(\lambda)\,e^{-\lambda t}\,d\lambda & t>0\end{cases}$$

which gives directly the consequence that

$$c(t)>0 \quad \text{for } 0<t<\infty.$$

This constraint that the function be a positive real function has applications in many branches of physics, for example, that the Laplace transform of a linear network driving-point-impedance be a positive real function is one of the necessary conditions in order for it to be realized as a Brune or Bott-Duffin network (Ferris 1962).

Further restrictions on the necessary form of $c(t)$ may be derived by differentiating $c(t)$ with respect to time. This yields that in the range $0<t<\infty$,

$$c'(t)<0, \quad c''(t)>0, \quad c'''(t)<0$$

etc.

These conditions on the sign, slope and curvature result in a very strong constraint on the permitted form of the earth's inductive impulse response function, $c(t)$.

3. Determination of $C(\omega, k)$

To determine $C(\omega, k)$ from Eq. (1), it is necessary to derive the spatial gradients of the horizontal field component at each frequency. This was accomplished in this work by fitting a second order 2D polynomial of the form

$$H(x,y)=h_0+h_1x+h_2y+h_3x^2+h_4y^2+h_5xy+\delta H_x \tag{15}$$

(similarly for D and Z), to the real and imaginary parts of each of the 3 components at each Fourier harmonic. (Note: to ease notation, the forms $H_x\equiv H$, $H_y\equiv D$ and $H_z\equiv Z$ have been used.) This is exactly the same procedure as that adopted in a similar analysis by Woods and Lilley (1979).

However, in order to determine surfaces which were as physically meaningful as possible, the solutions were constrained to be curl-free, that is

$$\frac{\partial H_x}{\partial y}=\frac{\partial H_y}{\partial x}$$

thus permitting no vertical current flow, $j_z=0$.

This causes a coupling of the surfaces for (H, D) because

$$h_2=d_1,$$
$$2h_4=d_5,$$
$$h_5=2d_3,$$

must be upheld for a curl-free solution. Hence, the two independent equations for H and D of 6 complex unknowns each, are reduced to a combined form of 9 complex unknowns. This necessitates information from a minimum of 5 stations, each station contributing 4 degrees of freedom to the solution, the locally observed real and imaginary parts of the two horizontal components.

The spatial gradient terms at the origin are hence

$$\frac{\partial H_x}{\partial x}\triangleq h_1$$
$$\frac{\partial H_y}{\partial y}\equiv d_2$$

and the denominator in Eq. (1) is (h_1+d_2).

For the value of $H_z(\omega)$, 2D surfaces of the form of (15) were also fitted to the observed vertical fields. This was because what is being attempted by this method is the derivation of a parameter that permits interpretation in terms of a *regional* 1D conductivity-depth distribution, and not one that is grossly perturbed by *local* induction anomalies. In this respect, the vertical magnetic field component observed at any one location may not truly reflect the regional field, but may be – and often is – highly indicative of more local structure. Hence, to try to remove this local effect at the central point of the investigation area, the observed H_z variations were also fitted by the polynomial of form (15). Thus, the numerator in Eq. (1) is (z_0).

One very important consequence of representing the field by a polynomial of second order is that the relationship (1) reduces to

$$C(\omega,0)=\frac{\tilde{H}_z}{\frac{\partial}{\partial x}\tilde{H}_x+\frac{\partial}{\partial y}\tilde{H}_y}$$

(Weidelt 1978, 142–143), where $\tilde{H}(x,y,0)$ is the magnetic field determined from fitting equations of the form (15). Thus, the derived inductive response function can be interpreted without regard to non-uniform source field configuration, and is henceforth written as $C(\omega)$.

Three techniques were compared to determine estimates of $C(\omega)$ from the derived horizontal spatial gradient and smoothed vertical field terms.

Method 1. At each Fourier harmonic, j, the raw inductive response function $C_j(\omega)$ was derived from

$$\hat{C}_j=\frac{(z_0)}{(h_1+d_2)} \tag{16a}$$

(dependence on frequency assumed). These $\hat{C}_j$'s were then band-averaged to give a smoothed $\bar{C}_1$ with the acceptance criteria that, for each estimate, inequalities (8a) and (8b) be upheld, i.e., Real $(\hat{C}_j)\geqq 0$ and Imaginary $(\hat{C}_j)\leqq 0$. Hence, estimate (1) is given by

$$\bar{C}_1(\bar{\omega})=\langle C_j(\omega)\rangle. \tag{16b}$$

Method 2. The raw estimates of numerator and denominator of Eq. (1) were frequency band-averaged, and the smoothed $\bar{C}_2$ was given by

$$\bar{C}_2(\bar{\omega})=\frac{\langle(z_0)\rangle}{\langle(h_1+d_2)\rangle}\ . \tag{17}$$

Method 3. Equation (1) describes a linear system with an input related to an output by an impulse response function, or, in the frequency domain, a frequency response function. This is illustrated in Fig. 1. In this formalism, Eq. (1) can be considered exactly as Eq. (6) with

$$I(\omega)\equiv\frac{\partial H_x(\omega)}{\partial x}+\frac{\partial H_y(\omega)}{\partial y}, \tag{18a}$$

$$O(\omega)\equiv H_z(\omega), \quad \text{and} \tag{18b}$$

$$H(\omega)\equiv C(\omega) \tag{18c}$$

Eq. (5) may be solved by method of cross-spectral analysis invoking the Wiener-Hopf integral equation and the Wiener-Khintchine theorem, to derive the least-squares estimate of $H(\omega)$. However, as shown in Jones (1980), there exist two possible forms of the least-squares estimate. Form (1) is

$$\bar{C}_L(\bar{\omega})=\frac{S_{io}(\bar{\omega})}{S_{ii}(\bar{\omega})} \tag{19}$$

where $S_{ab}(\bar{\omega})=\langle A^*(\omega)B(\omega)\rangle$, i.e., the cross-spectra between $A(\omega)$ and $B(\omega)$, and is *downward-biased* for noise occurring on the input, i.e., the spatial gradient term (18a). Form (2) is

$$\bar{C}_U\ (\omega)=\frac{S_{oo}(\bar{\omega})}{S_{oi}(\bar{\omega})} \tag{20}$$

and is *upward-biased* for noise occurring on the output, i.e., the smoothed vertical magnetic field term (18b). The smoothed $\bar{C}_3$ estimate was given by

$$\bar{C}_3(\bar{\omega})=\frac{\bar{C}_L(\bar{\omega})+\bar{C}_U(\bar{\omega})}{2}. \tag{21}$$

Estimate $\bar{C}_3(\bar{\omega})$ is itself only unbiased by noise contributions if the input signal-to-noise ratio exactly equals the output signal-to-noise ratio (Jones 1980). The true unbiased response function lies in the interval $(C_L,\ C_U)$.

The estimate of the coherence between the input and output of a single input – single output linear system, in this case between the horizontal spatial gradients and the vertical magnetic field, is given by

$$\hat{\gamma}^2_{io}(\bar{\omega})=\frac{|S_{io}(\bar{\omega})|^2}{S_{ii}(\bar{\omega})S_{oo}(\bar{\omega})}\ . \tag{22}$$

However, this estimate is relatively well known to be a biased function. For example, although the *true* coherence between two random data sets is zero, the *estimate* of the coherence is non-zero due to the bias associated with the cross-spectral estimate, $S_{io}(\bar{\omega})$. The expectation value of the estimate of the ordinary coherence function between two random data sets is

$$E[\hat{\gamma}^2_{r_1r_2}]=\frac{2}{n}$$

where n is the number of degrees of freedom associated with the smoothed spectral value (each Fourier harmonic has two degrees of freedom, one for the real and one for the imaginary part). Jones (1977, 1979) suggested a method of correcting for this bias by normalising the coherence value after transforming the function into a domain where it exhibits a normal distribution. This normalised transformed ordinary coherency function, N_{xy}, given by

$$\hat{N}_{xy}=\frac{\tanh^{-1}(\hat{\gamma}_{xy})}{\tanh^{-1}((2/n)^{1/2})} \tag{23a}$$

has a variance of

$$\sigma^2_{N_{xy}}=\frac{1}{n\,\mathrm{arctanh}^2((2/n)^{1/2})}, \tag{23b}$$

where $\hat{\gamma}_{xy}$ is the estimated ordinary coherency [the positive square root of the estimated ordinary coherence given by (22)],

and n is the number of degrees of freedom associated with the estimate,

and there is an expectation value of

$$E[\hat{N}_{xy}]=1,$$

for random data sets.

The derived inductive response function from (21), $\bar{C}_3(\bar{\omega})$, is only an estimate of the true response function, $C(\omega)$, and it can be shown that, if the total noise terms constitute a white series, then a confidence region for $C(\omega)$ can be specified at a confidence level of $100(1-\alpha)\%$ from

$$|\bar{C}_3(\bar{\omega})-C(\omega)|^2\ \leqq\frac{2}{n-2}F_{2;n-2;1-\alpha}(1-\hat{\gamma}^2_{io}(\bar{\omega}))\,\frac{S_{oo}(\bar{\omega})}{S_{ii}(\bar{\omega})} \tag{24}$$

(see, for example, Bendat and Piersol 1971, 199–203), where $F_{2;n-2;1-\alpha}$ is the Fisher likelihood function with a $(1-\alpha)$ confidence coefficient,

$S_{oo}(\bar{\omega})$ is the smoothed estimate of the autospectra of the output, defined by (18b),

$S_{ii}(\bar{\omega})$ is the smoothed estimate of the autospectra of the input, defined by (18a),

and $\hat{\gamma}^2_{io}(\bar{\omega})$ is the estimate of the coherence function between the input and the output, given by (22).

4. Application

The application of this method is only worthwhile if interpretable response functions are determined. In this respect, the *major* assumption made is that the observed magnetic fields result from induction by a non-uniform source over an earth which

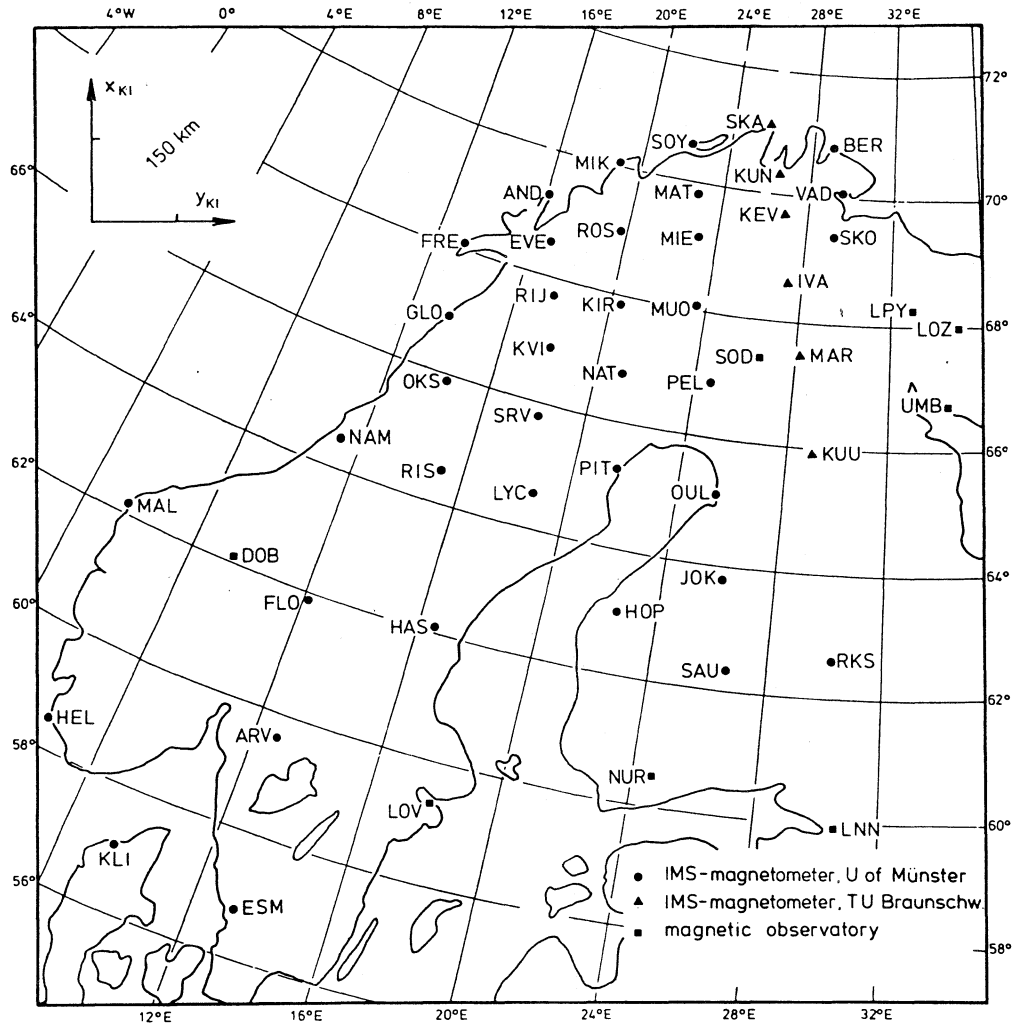

Fig. 2. Station map in geographic coordinates. Also indicated are the axes of the Kiruna cartesian coordinate system (see Küppers et al. 1979)

has a 1D conductivity distribution, i.e., that conductivity is a function of depth only, $\sigma(z)$.

In following papers, it will be illustrated that the region around Kiruna (KIR) (see Fig. 2) displays small anomalous induction effects, and that magneto-telluric data recorded at Nattavaara (NAT) exhibits, to a first approximation, one-dimensionally. Hence data from the zone centered on Kiruna should be interpretable in terms of a 1D structure. The nearest obvious 2D or 3D structure is the coast, which is more than 300 km from Kiruna.

The principal reasons for the operation of the array were coordinated observations with other groups of the ionospheric current systems for the International Magnetospheric Study (Küppers et al. 1979). Hence many events of profoundly different current configurations were digitised for analysis (see for example Baumjohann et al. 1978, 1980; Mersmann et al. 1979; Untiedt et al. 1978; and Küppers et al. 1979). Some of these have proved suitable for determination of $C(\omega)$ due to the strong spatial gradients observed.

As an example, consider the magnetogram illustrated in Fig. 3. This is a record of the magnetic field variations recorded by the Kiruna (KIR, Fig. 2) magnetometer between 15:00 UT and 23:00 UT on 2 December 1977. This event is of special world-wide interest as it occurred during a very favourable configuration of three different satellites. Study of the event has inferred extremely complex auroral zone current structure over Scandinavia during the interval.

The magnetic data from the stations EVE, RIJ, KVI, SRV, ROS, KIR, NAT, MIE, MUO, and PEL (Fig. 2) were digitised, conditioned and fast Fourier transformed to give the raw Fourier harmonics at each station. Each time series was of 2,880 points with a sampling interval of 10 seconds which was extended by zeroes to 4,096 giving 2,049 harmonics, each harmonic having 1.4 degrees of freedom (0.7 each for the real and imaginary parts respectively).

Using the procedures outlined in Sect. 3, the fields were fitted by polynomials at each Fourier harmonic. The fit was by least-squares methods which minimised the Euclidean norm between the solutions of the overdetermined system (Golub 1965), i.e., minimised $|\delta H_x + \delta H_y|^2$ and $|H_z^2|$ for the horizontal and vertical field solutions respectively. The 10 stations employed give 40 degrees of freedom for the horizontal field and 20 for the vertical field. The polynomials require 18 and 12 degrees of freedom for the horizontal and vertical solution respectively. Hence the combined horizontal field solution has 22 degrees of freedom whilst that of the vertical field has 8 degrees of freedom.

The estimates of C for the three different methods described in Sect. 3 were frequency band averaged with a constant Q filter

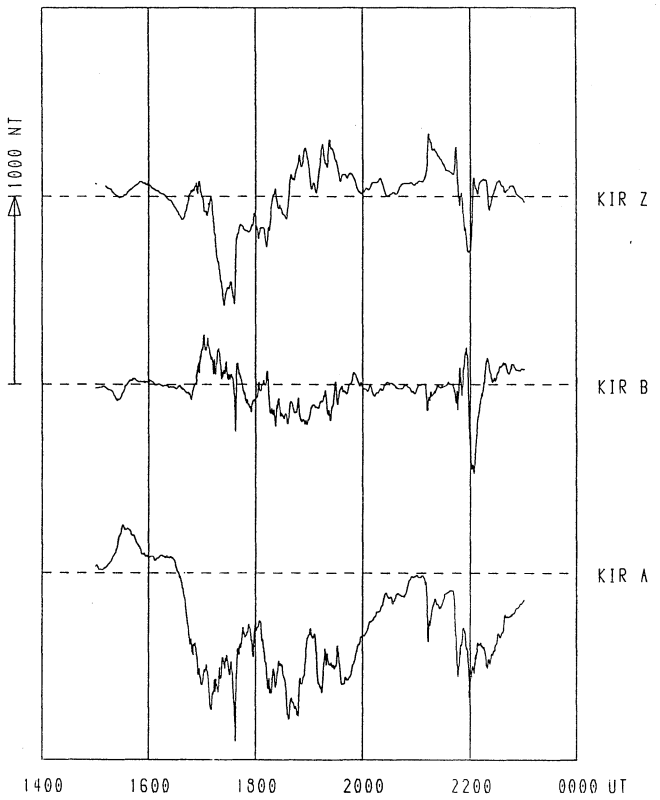

Fig. 3. Magnetic data recorded at Kiruna in the interval 15:00–23:00 UT on 2nd December 1977. *A*, component toward north; *B*, toward east, *Z*, vertically downwards

of box-car form with $Q=0.5$. These solutions for g and h (where $C=g-ih$) are illustrated in Fig. 4a and 4b respectively. It is apparent from these figures that method 3, employing statistical frequency analysis techniques, produces far smoother estimates than either of the other two methods.

In Fig. 5 are displayed the downward-biased and upward-biased estimates, from Eqs. (19) and (20) respectively, of $C_3(\omega)$, together with the 95% confidence intervals, calculated from (24). It is apparent from the figure that there is little bias due to noise in the estimates, but, at long periods, the confidence intervals are large. In Fig. 6 is displayed the coherence function between the input and output of the system, and also the normalised transformed ordinary coherency, as defined by (23a), N_{i_o}. The two series appear well correlated, even at short periods of the order of hundreds of seconds.

A total of 8 events were analysed in the manner described above, and the individual estimates for g and h were averaged in a weighted manner by the algorithm

$$\bar{g}(\bar{\omega}_j)=\frac{\sum_{i=1}^{8} N_i(\bar{\omega}_j)\cdot g_i(\bar{\omega}_j)}{\sum_{i=1}^{8} N_i(\bar{\omega}_j)} \tag{25}$$

similarly for $\bar{h}(\bar{\omega}_j)$. The sample weighted variances of the estimates were determined using the algorithm which gives an efficient and consistent unbiased estimate

$$s_g^2=\frac{n}{n-1}\,\frac{\sum N_i(g_i-\bar{g})^2}{\sum N_i} \tag{26}$$

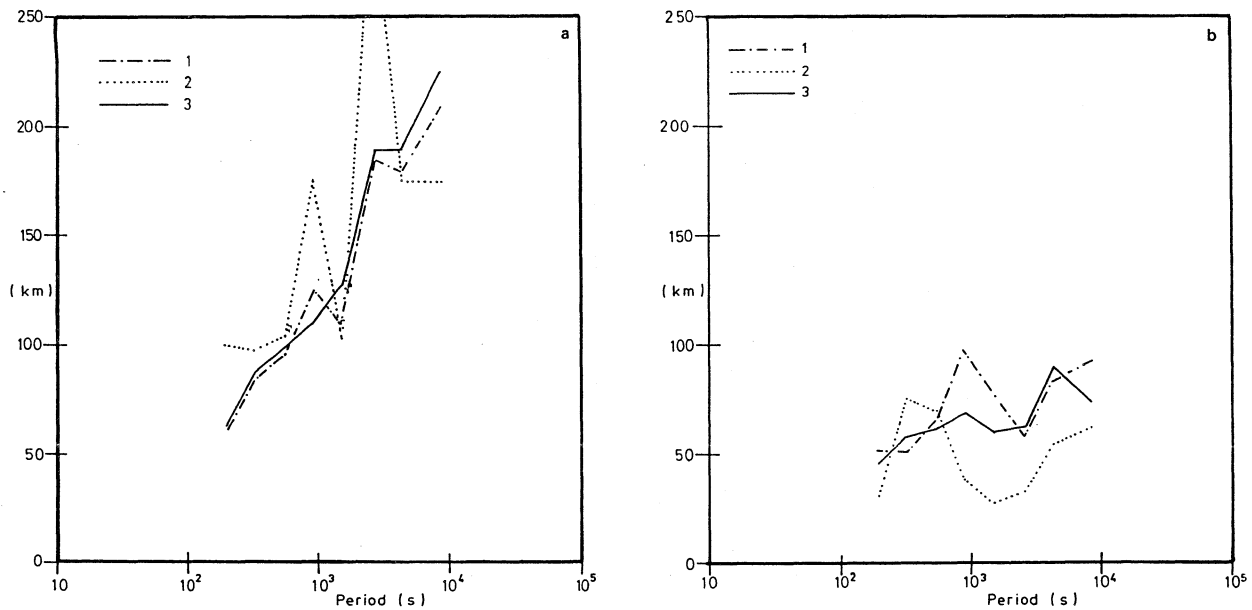

Fig. 4. a Determinations of g from the three methods outlined in Sect. 3; (-·-·-) method 1, (·····) method 2, (———) method 3. **b** As for (**a**) but for h

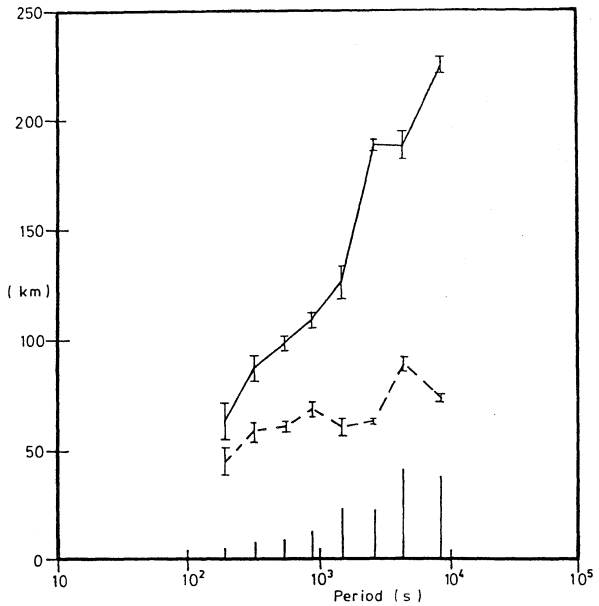

Fig. 5. The estimates from method 3 for g (*full line*) and h (*dashed line*) showing the downward- and upward-biased estimates as error bar ranges. The 95 % confidence intervals are given by the magnitude of the *solid lines* at the base of the figure

(dependence on frequency assumed)

where s_g^2 – is the sample weighted variance of the estimate $\bar{g}$
n – number of estimates
N_i – the function, as defined by (23a) for the i'th estimate
g_i – the i'th estimate of g
$\bar{g}$ – the weighted average, given by (25)

similarly for s_h^2.

Variances, and their square root, the standard deviation, are in themselves very weak statistical parameters. They only describe the dispersion, or scatter, of the individual estimates which are employed to determine the mean value. A far more powerful statistical description is given by the confidence intervals, at a certain probability level, of the determined mean values. Because the true weighted variance, σ^2, is unknown and is only estimated by the sample weighted variance, given by (26), statements regarding possible future values of the sample weighted mean, from (25), must be made by employing the Student-t, rather than the normal, distribution. The probability that any mean, $\bar{x}$, will exceed the true mean, μ_x, plus an associated confidence interval, is given by

$$\text{Prob}\left[\bar{x} > \mu_x + \frac{s t_{n-1:\alpha}}{n^{1/2}}\right] = \alpha$$

where μ_x is the true mean
$\bar{x}$ is the sample (weighted) mean
s is the sample (weighted) standard deviation
$t_{n-1:\alpha}$ is the Student-t distribution at the α confidence level for $(n-1)$ degrees of freedom
α is the probability level
and n is the total number of degrees of freedom.

Accordingly, the $100(1-2\alpha)\%$ confidence intervals for $\bar{x}$ are given by

$$\left(\bar{x} - \frac{s t_{n-1:\alpha}}{n^{1/2}}\right) \leqq \mu_x \leqq \left(\bar{x} + \frac{s t_{n-1:\alpha}}{n^{1/2}}\right). \tag{27}$$

Figure 7a and b display the individual estimates of $g_i(\bar{\omega})$ and $h_i(\bar{\omega})$ from the 8 events, with their relative weighting being crudely indicated by the type of symbol used.

The weighted means, from (25), are joined by the full lines, and the relative 95 % confidence intervals for these means from (24) and (25) are also shown. These mean values have been further smoothed by a Hanning window, $(\frac{1}{4}, \frac{1}{2}, \frac{1}{4})$, to give the dashed lines indicated in Fig. 7a and b and given in Table 1 together with the confidence intervals.

The statistical method described above for determining the means, and the confidence limits of those means, of the parameters $\bar{g}$ and $\bar{h}$ only necessitates assuming that for these data the Central Limit Theory is valid, i.e., that the probability density functions of the estimates of g and h tend very quickly to the Normal form as the number of estimates is increased. This is a very weak statistical assumption to make when compared to that made for determining confidence intervals from equations

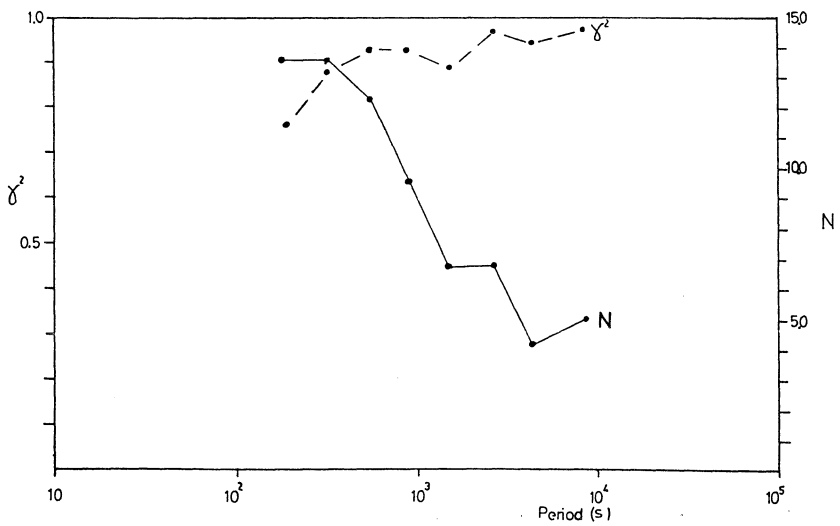

Fig. 6. Coherence functions between the derived vertical field and spatial gradient of the horizontal field; (– – –) γ^2, usual ordinary coherence function; (——) N, normalised transformed ordinary coherency function

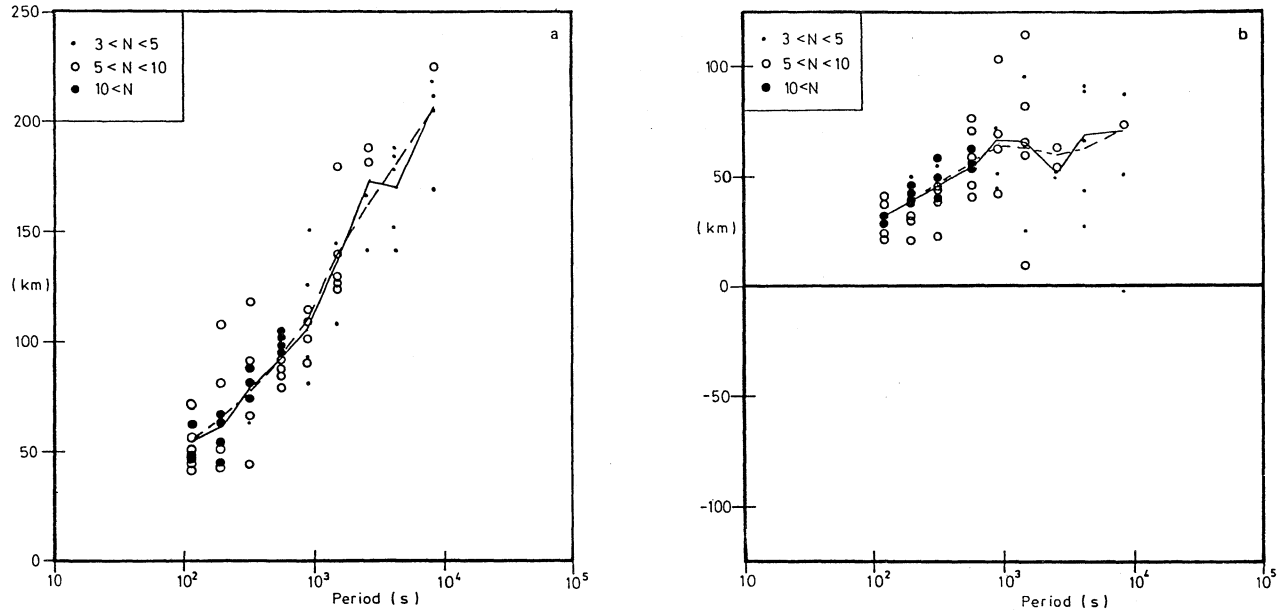

Fig. 7. a Individual event determinations of g with the corresponding value of the normalised transformed ordinary coherence being indicated by symbol type: $\bullet \equiv 3 < N < 5$; $\circ \equiv 5 < N < 10$; $\bullet \equiv 10 < N$. The *full line* indicates the weighted ensemble average, and the *dashed line* is the Hanning-smoothed average. **b** As (**a**) but for h

Table 1. Determined response function and confidence intervals

Period(s)	$\bar{g}$ (km)	$\bar{h}$ (km)	r_g (km)	r_h (km)	ρ_a (Ωm)	ϕ_a(degrees)
115	55.2	31.5	9.2	4.9	277	60
190	64.2	38.6	15.6	6.7	231	60
320	77.7	47.6	15.0	7.8	204	58
535	92.4	57.5	6.2	8.7	175	58
890	110.6	63.6	16.0	17.0	144	61
1,490	138.0	62.7	19.6	41.5	122	66
2,480	163,0	60.0	32.7	9.5	96	70
4,090	179.7	63.8	25.6	35.0	70	70
8,200	206,0	71.5	37.9	42.0	46	71

$\bar{g}$ and $\bar{h}$ are the smoothed real and imaginary parts of the response function, averaged over eight independent events

r_g and r_h are the 95 % confidence intervals of the parameters $\bar{g}$ and $\bar{h}$ respectively

ρ_a and ϕ_a are the apparent resistivity and phase of the derived inductive response function

of the form (24). This method also has another advantage over the more usual statistical technique, of, for example, averaging the ensemble estimates of (H_z) and $(\partial H_x/\partial x + \partial H_y/\partial y)$, in that higher weighting can be given to those estimates of $C_i(\omega)$ which are considered more superior (Eq. (25)).

5. Validity

Having obtained the smoothed values of $\bar{C}(\bar{\omega})$, as displayed in Fig. 7a and b and given in Table 1, there are certain questions that can be posed regarding the validity of the inductive response function so determined.

5.1. *Does the Function Describe a Causal System?*

As detailed in Sect. 2.2, there are two tests which may be applied to determine whether or not the estimated response function describes a physically realisable, i.e., causal, linear system. It is known that at the periods of interest, 10^2–10^5 s, the Earth responds inductively in a causal manner. Hence any response function that describes the induction process must comply to conditions (5), (7a), and (7b).

5.1.1. Is $c(t)=0$ for $t<0$? Defining the forward Fourier transform operator by $\mathcal{F}$, given by

$$X(\omega) = \mathcal{F}\{x(t)\} = \int_{-\infty}^{\infty} x(t)\, e^{-j\omega t}\, dt \tag{28a}$$

and the inverse Fourier transform operator by $\mathcal{F}^{-1}$,

$$x(t) = \mathcal{F}^{-1}\{X(\omega)\} = \frac{1}{2\pi} \int_{-\infty}^{\infty} X(\omega)\, e^{j\omega t}\, d\omega \tag{28b}$$

it is easy to prove that

$$x(-t) = \mathcal{F}\{X(\omega)\} = \frac{1}{2\pi}\, \mathcal{F}\mathcal{F}\{x(t)\}$$

(Champeney 1973). If $x(t)$ is a purely real series, then from symmetry relations

$$x(-t) = \mathcal{F}^{-1}\{X^*(\omega)\} \tag{29}$$

where $X^*(\omega)$ is the complex conjugate of (28a).

Hence, for a response function, the inverse Fourier transform gives the impulse response function for all positive lags, and the inverse Fourier transform of the complex conjugate of the

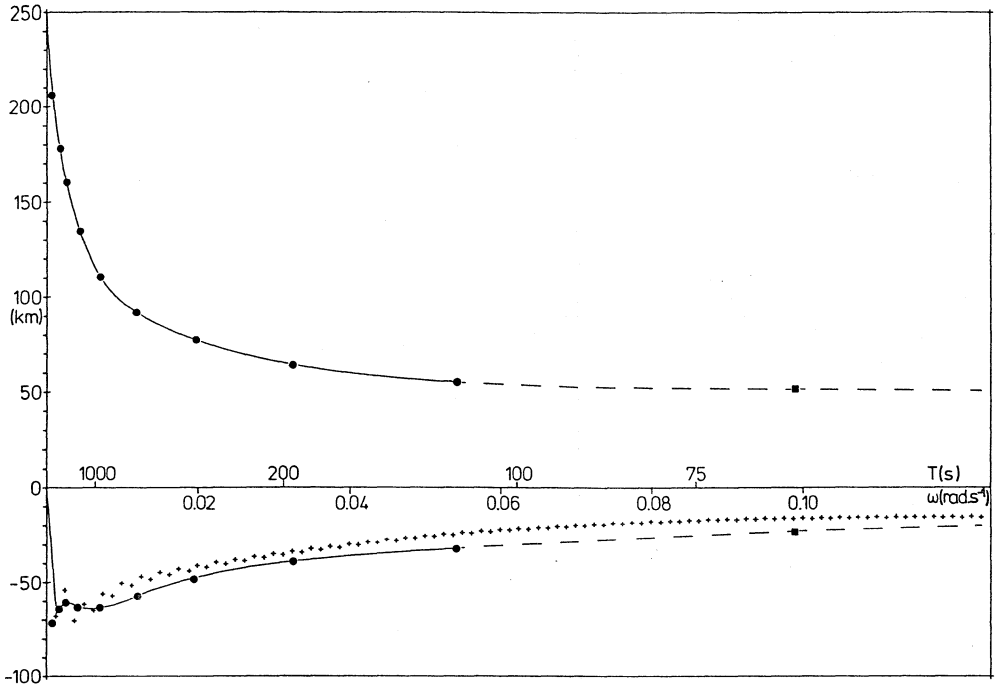

Fig. 8. Interpolation of g (positive) and $-h$ (negative) in the observation range given by *solid lines*. *Dashed lines* are the extrapolations of these functions to higher frequencies using the parameters from a two-layer model as aids (*squares*). *Crosses* are the function $g_H = -\mathcal{H}\{g\}$, the Hilbert transform of g

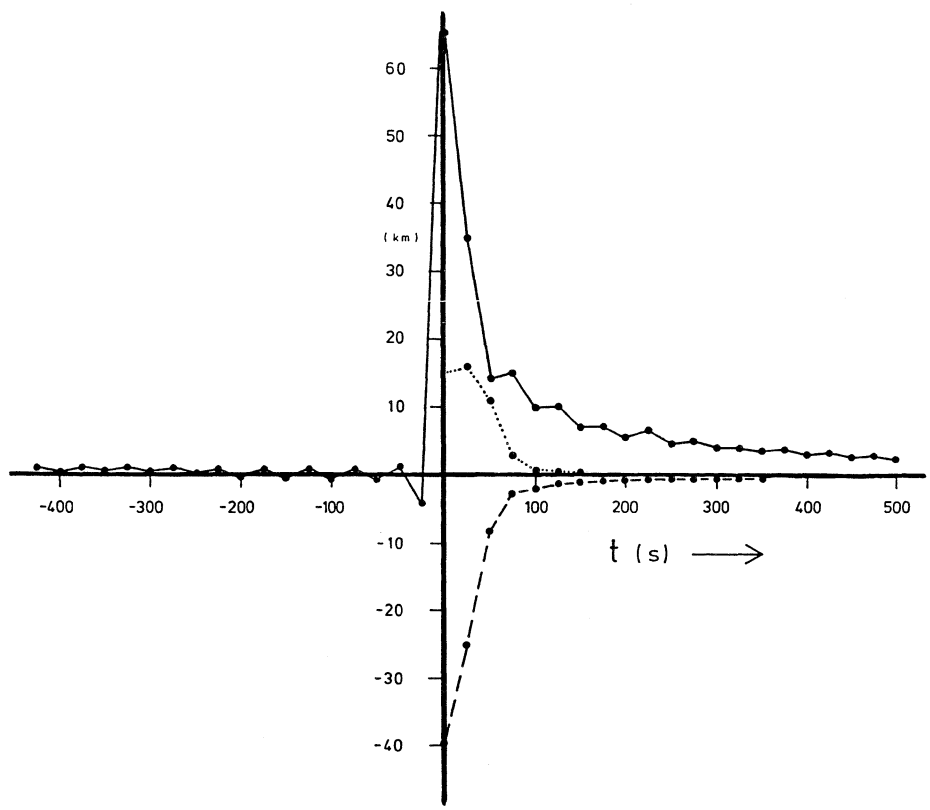

Fig. 9. Inductive impulse response function, $c(t)$ (————), with its first differential, $c'(t)$ (— — — —), and second differential, $c''(t)$ (·····), with respect to time

response function gives the impluse response function for all negative lags, i.e.,

$$c(\tau)=\begin{cases}\mathcal{F}^{-1}\{C(\omega)\} & \tau \geqq 0 \quad (30\,a)\\ \mathcal{F}^{-1}\{C^*(\omega)\} & \tau \leqq 0. \quad (30\,b)\end{cases}$$

The inductive response function given in Table 1 was interpolated by fitting cubic spline functions to give estimates which were equally spaced in the frequency domain. This fit is illustrated in Fig. 8. These values were then employed to derive the impulse response function $c(\tau)$, for both positive and negative

lags, by utilising expressions (30a) and (30b). The resulting impulse response function is illustrated in Fig. 9, from which it can be seen that the function does indeed comply with the requirement of a causal system that $c(\tau)=0$ for $\tau<0$.

5.1.2. Are the real and imaginary parts of $C(\bar{\omega})$ related by the Hilbert transform? There are two techniques for deriving the Hilbert transform of a function. The first is to evaluate the integral form directly, as expressed by Eq. (7a) and (7b), the second employs Fourier transformation. Both, however, require that the function be well described over a sufficiently long interval that the basic assumptions that have to be made regarding the function outside the interval be valid.

For $\omega=0$, then from (13)

$$h=0$$

and $$\lim_{\omega\to 0}(g)=\frac{1}{k}\tanh(kd).$$

Assuming kd are such that $\tanh(kd)\simeq kd$, then $g\simeq d$. For this, $kd\lesssim 0.5$ such that the wavelength, λ, of the field must be

$$\lambda>\pi\cdot d.$$

Hence reasonable values of d ensure $g\simeq d$ for the wavelengths of the fields analysed. A value of $d=250$ km was adopted.

At the very high positive frequencies, g and h tend towards expressions (13b) and (13d), i.e., the same values. Assuming that Scandinavia is overlain by a resistive top layer of about $10^4\,\Omega$m, which is inferred by the work of Westerlund (1972), of thickness at least 10 km, then the period at which this is the skin depth is given by

$$\delta=0.5(\rho T)^{1/2}$$

where δ is the skin depth in km
ρ is the layer resistivity in Ωm
and T is the period in seconds

and for $\delta=10$ km with $\rho=10^4\,\Omega$m gives $T=0.04$ s.

Hence, for $\omega>160$ rads^{-1} ($T<0.04$ s)

$$g(\omega)=h(\omega)=\frac{63}{\omega^{1/2}}\text{ km}$$

or

$$g(T)=h(T)=25\,T^{\frac{1}{2}}\text{ km}.$$

At the intermediate periods, $100<T<0.04$, it is necessary to assume a conductivity distribution in order to aid the interpolation of the data in this range. Using an algorithm given by Fischer and Schnegg (in press 1980), a two-layer model was derived which was compatible with the three shortest period $|\bar{C}(\bar{\omega})|$ values. This model consisted of a top layer of $10^4\,\Omega$m and thickness 30 km, underlain by a more conducting layer of 125 Ωm. These values are indicated in Fig. 8 where the solid lines are the interpolation using the derived values of $\bar{C}(\bar{\omega})$ (Table 1) and the dashed lines are the extrapolation constrained

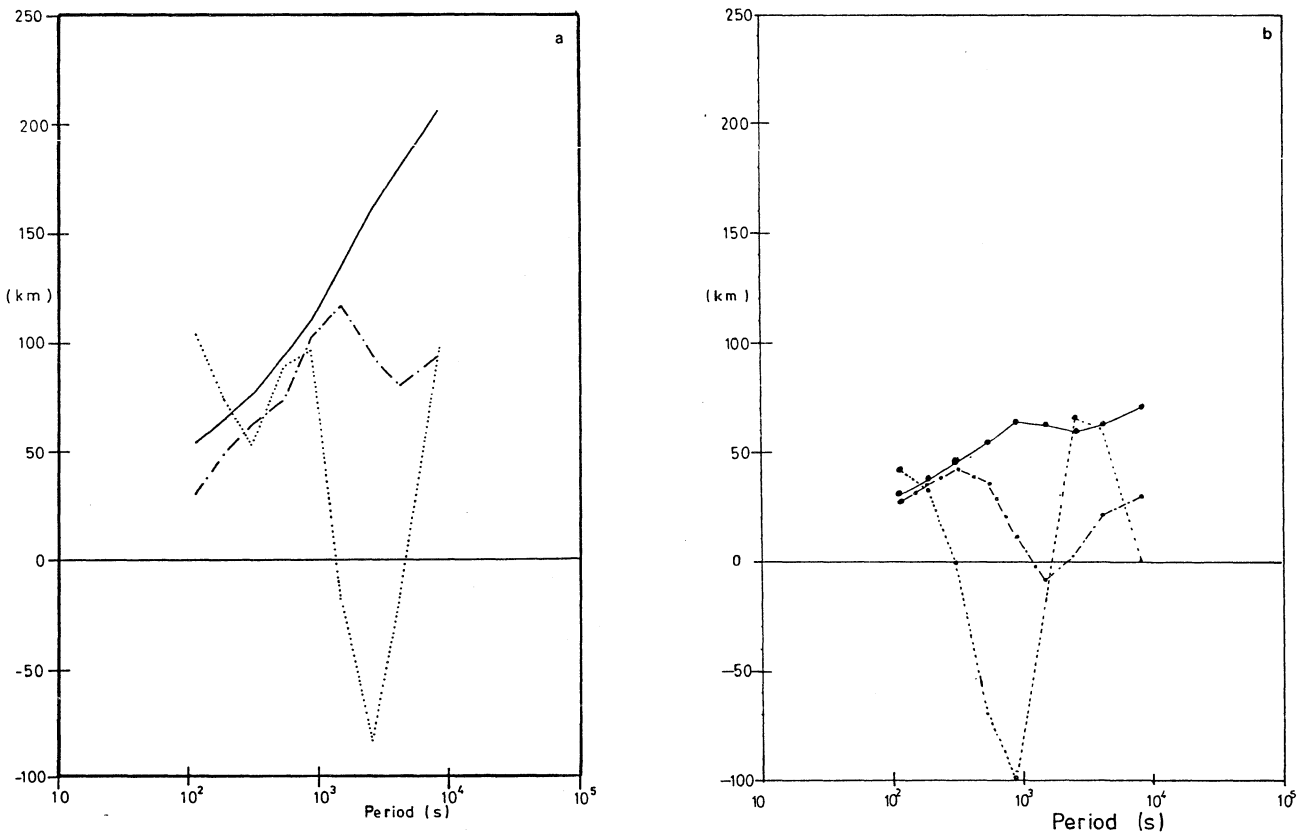

Fig. 10. a The function $g(\omega)$ (———) with its first derivative (- - -) and second derivative (·····) with respect to log T. **b** As 10a but for the function $h(\omega)$

Table 2. Tests of Weidelt's inequality constraints

Period	8a	8b	9	10a	10b	11a	11b	12a	12b
115	+	+	+	+	+	−	+	−	−
190	+	+	+	+	+	−	+	−	+
320	+	+	+	+	+	−	+	−	+
535	+	+	+	+	+	−	+	−	+
890	+	+	+	+	+	−	+	−	+
1,490	+	+	+	+	+	−	+	+	+
2,480	+	+	+	+	+	−	+	−	+
4,090	+	+	+	+	+	−	+	−	+
8,200	+	+	+	+	+	−	+	−	+

+ : the inequality was upheld by the response function
− : the inequality was not upheld by the response function

by the 2-layer 1 D model described above. Although these somewhat severe assumptions about the form of $\bar{C}(\bar{\omega})$ outside the observation interval have been made, it must be remembered that the kernel of the Hilbert transform integral possesses a simple pole at ω_0. Hence, any reasonable extrapolation of the function outside the interval will not seriously affect the transformation for values of ω_0 which are in the observation interval and not too close to the high and low frequency bounds.

Using the procedure for evaluating Hilbert transforms given by Čižek (1970), the real part of the inductive response function g, was Hilbert transformed in the range $0<\omega<0.628\,\mathrm{rad\,s^{-1}}$, where the necessary values for extrapolation were taken as described above. The derived function $g_H(\omega)=-\mathscr{H}(g(\omega))$ is also displayed in Fig. 8 where a very good correlation between it and $-h(\omega)$, i.e., the imaginary part of $\bar{C}(\bar{\omega})$, in the range $0.015<\omega<0.040\,\mathrm{rad\,s^{-1}}$ can be seen. The underestimate of the function $g_H(\omega)$ is possibly an artifact of the enforced cut-off of the slowly decaying function $g(\omega)$ at high frequencies.

This comparison also gives much weight to the argument that the values determined for the function $C(\omega)$ describe a *physically realisable* system.

5.2.1. Do the estimates of $C(\omega)$ comply with the inequality constraints? Weidelt (1972) lists 22 inequality constraints imposed on $C(\omega)$, 9 of which are given here by Eqs. (8)–(12). In order to discover if the estimates of $C(\omega)$ satisfy these 9 constraints, the two curves for $g(T)$ and $h(T)$ were differentiated by determining the derivative of the Lagrangian interpolation polynomial of degree 2 relevant to the three neighbouring values of g_i and h_i on a logarithmic period scale (Hildebrand 1956).

The derivatives $\partial g/\partial(\log T)$ and $\partial h/\partial(\log T)$ are illustrated, together with $g(T)$ and $h(T)$, in Figs. 10a and b respectively. The second derivatives $\partial^2 g(T)/\partial(\log T)^2$ and $\partial^2 h(T)/\partial(\log T)^2$ were derived by differentiating, in a similar manner, the first derivatives. These are also illustrated in Figs. 10a and b. The constraints given in Eqs. (8)–(12) were tested for, and the results are compiled in Table 2. It is apparent from Table 2 that inequalities (11a) and (12a), viz.

$$|DC|\leqq h, \quad |D^2 C|\leqq h$$

are not upheld at any period, with the one exception of (12a) at 1490 s. This was also found to be fairly consistently true of all the individual event estimates of $C(\omega)$, whereas the other constraints were, in general, upheld. This is taken as an indication that the data are not totally consistent with a 1 D Earth conductivity-depth distribution model, but arise from effects due to 2- or 3-dimensionality. However, it is believed that a 1 D model is a good approximation.

5.2.2. Does $c(t)$ Display the Required Form? As described in Sect. 2.3 (see acknowledgements for reference), the inductive impulse response function, $c(t)$, given by the inverse Fourier transform of $C(\omega)$, i.e., $c(t)=\mathscr{F}^{-1}\{C(\omega)\}$, must display the form

$$c(t)>0,\ c'(t)<0,\ c''(t)>0 \quad \text{for } 0<t<\infty.$$

The estimated function $c(t)$, illustrated in Fig. 9, is certainly a positive function in the range $t>0$, and differentiation of this function, undertaken in the same manner as described in 5.2.1, showed that the above conditions on the gradient and curvature of $c(t)$ are also fully upheld (Fig. 9). These three requirements on the form of $c(t)$ are a very strong constraint imposed on it, and that they are all displayed by the estimate determined is a powerful indication that $\bar{c}(t)$, and hence $\bar{C}(\bar{\omega})$, is interpretable in terms of the conductivity structure under northern Sweden.

6. Implications

A full interpretation of the geomagnetic and magneto-telluric results will be presented in a later paper in this series. However, it is considered worthwhile to examine the implications of the determined $\bar{C}(\bar{\omega})$ function in a preliminary manner here.

The ρ^*-z^* inversion of the $\bar{C}(\bar{\omega})$ data listed in Table 1 is shown, with the 95 % confidence limits, in Fig. 11. The data show a clear trend towards a more conducting layer at depth. Also included in the figure is the two-layer model determined from the first three points, using the algorithm of Fischer and Schnegg (in press 1980), and the preliminary results of a Monte-Carlo inversion, of the type proposed in Jones and Hutton (1979), of the magneto-telluric data recorded at Nattavaara (NAT, see Fig. 2) in northern Sweden, some 120 km south of Kiruna (Jones and Olafsdottir 1979).

The apparent resistivity and phase data, derived from

$$\bar{\rho}_a(\bar{\omega})=\omega\mu_0|\bar{C}(\bar{\omega})|^2,$$

$$\bar{\phi}_a(\bar{\omega})=-\tan^{-1}\left(\frac{\mathrm{Re}(\bar{C}(\bar{\omega}))}{\mathrm{Im}(\bar{C}(\bar{\omega}))}\right)$$

is shown in Fig. 12. A 3-layer 1 D model of parameters $\rho_1=10^4\,\Omega$m; $\rho_2=125\,\Omega$m; $\rho_3=3.5\,\Omega$m; $d_1=30$ km; $d_2=140$ km, is also illustrated. Although the correspondence between the data and the theoretically calculated values is not good, the essential features of a resistive upper layer of about $10^4\,\Omega$m underlain by a layer of some 100 Ωm, with a highly conducting basement at a depth of around 140 km are well described.

7. Source Field Effects

In this work, the inductive response function $C(\omega,0)$ has been explicitly derived in a strict manner due to fitting the observed fields to a second order polynomial. Thus, it is not necessary to consider the effects of non-uniform source fields on the derived function when interpreting the data. Other methods may derive response functions which are however affected by the non-uniformity of the source field, for example, standard magneto-telluric analysis ($Z(\omega,k)$), the internal-external field ratios ($S(\omega,k)$), or functional representations of the field other than a

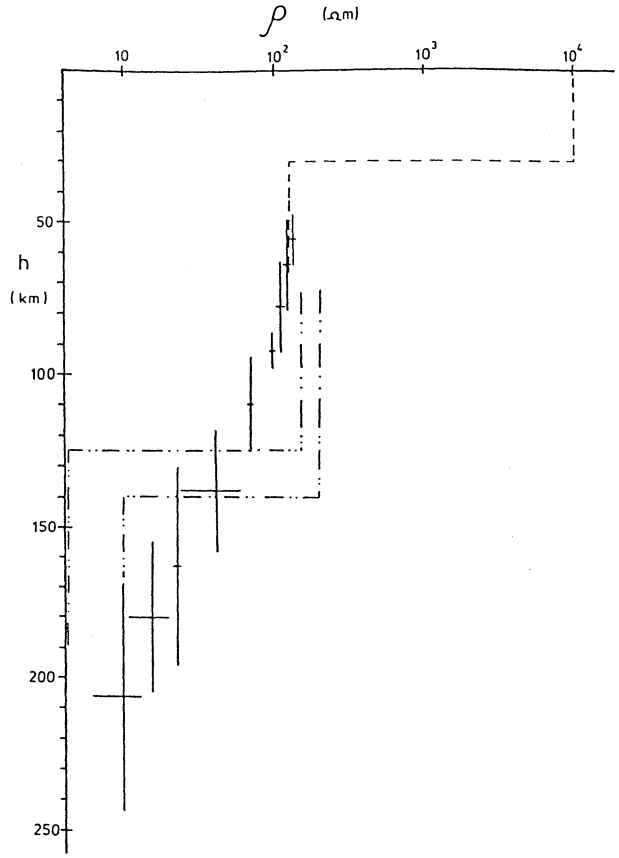

Fig. 11. The Schmucker ρ^*-z^* inversion of the derived function with corresponding 95 % confidence intervals. Also shown in the Fischer-Schnegg two-layer inversion (- - -) of the first three data points and the bounds of the Monte-Carlo inversion (-·····) of the long period magneto-telluric data recorded at NAT (see Fig. 2)

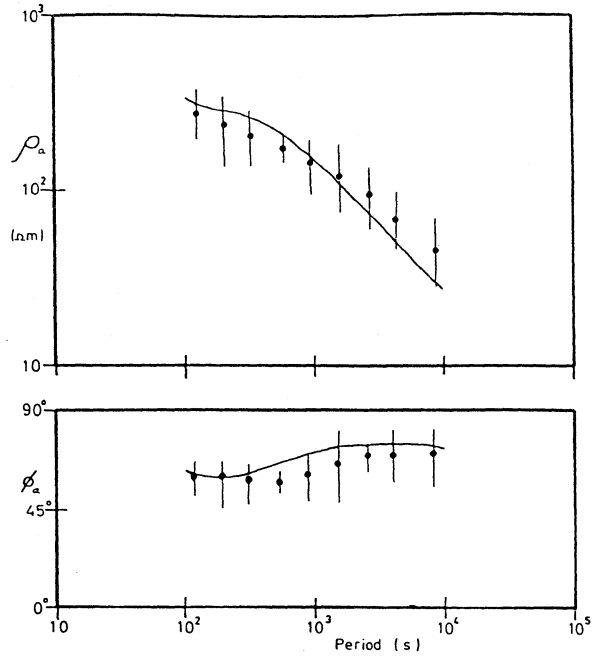

Fig. 12. The fit of a theoretical model of parameters: $\rho_1=10^4\,\Omega$m; $\rho_2=125\,\Omega$m; $\rho_3=3.5\,\Omega$m; $d_1=30$ km; $d_2=140$ km; to the derived inductive response function, expressed in terms of apparent resistivity and phase (*dots*), both with associated 95 % confidence limits shown

second-order polynomials in order to derive $C(\omega,k)$ from the HSG method. Hence, it is considered a worthwhile exercise to investigate the effects on $C(\omega,0)$ of non-zero values of wavenumber for the derived one-dimensional conductivity model, consistent with the magnetic data observed in northern Sweden.

As was shown by Price (1962) and Srivastava (1965), the effect of a non-uniform source field is to change the layer propagation constant from k_i, where k_i is given by

$$k_i=k_i(\omega,0)=\left(\frac{\omega\mu_i\sigma_i}{2}\right)^{1/2}+j\left(\frac{\omega\mu_i\sigma_i}{2}\right)^{1/2}$$

$k(\omega,0)$-uniform field propagation constant in the i'th layer μ_i-magnetic permeability of the i'th layer, σ_i-conductivity of the i'th layer

to a value of

$$k_i(\omega,k)=\frac{1}{2^{\frac{1}{2}}}(([|k_i(\omega,0)|^4+k^4]^{1/2}+k^2)^{1/2}$$
$$+j([|k_i(\omega,0)|^4+k^4]^{1/2}-k^2)^{1/2})$$

where $k=2\pi/\lambda$ and is the Price wavenumber.

The correction only becomes important for k of the order of $|k_i(\omega,0)|$. For the three layers of the model proposed in Sect. 6, and for the longest period of interest [i.e., the smallest possible value of $k_i(\omega,0)$], the following hold:

layer 1 $k\sim|k_1(\omega,0)|$ when $\lambda\sim10^4$ km,
layer 2 $k\sim|k_2(\omega,0)|$ when $\lambda\sim10^3$ km,
layer 3 $k\sim|k_3(\omega,0)|$ when $\lambda\sim200$ km,

hence the uppermost highly resistive layer is very sensitive to non-uniform fields. Figure 13 illustrates the effects of finite wavelengths on the parameters g and h. As can be seen from the figure, wavelengths of the order of 2×10^3 km or greater do not seriously affect g and h for periods less than 10^4 s.

Representation of the source configuration by a wavenumber, k, implicitly assumes, analogously to Fourier transformation, that the source is repeated in form every λ (wavelength $\lambda=2\pi/k$). This approximation is valid directly underneath an electrojet maximum, where the effective wavelength, λ_{eff}, is equal to four times the electrojet half-width, but becomes increasingly worse with distance away from the maximum. Using the programme of Hibbs and Jones (1976a, b), the variation of $C(\omega)$ with distance away from the centre of a Gaussian-shaped electrojet of half-width 500 km over the Earth model proposed in Sect. 6 was calculated and is also illustrated in Fig. 13. As can be seen by the spread of the determined g and h functions, under the centre of the electrojet $\lambda_{\text{eff}}=2{,}000$ km $=4\times$ half-width. Moving away from the centre, $\lambda_{\text{eff}}=\infty$ at the point directly underneath the half-width (i.e. ±250 km). Moving yet further away gives values *greater than* those for $k=0$, this arises because the effective wavenumber is complex.

The sources in Scandinavia are, as a rule, moving rather than stationary. As shown by Hermance (1978), this feature aids the magneto-telluric relationship, and hence correspondingly the inductive response function, in that a moving source has a larger

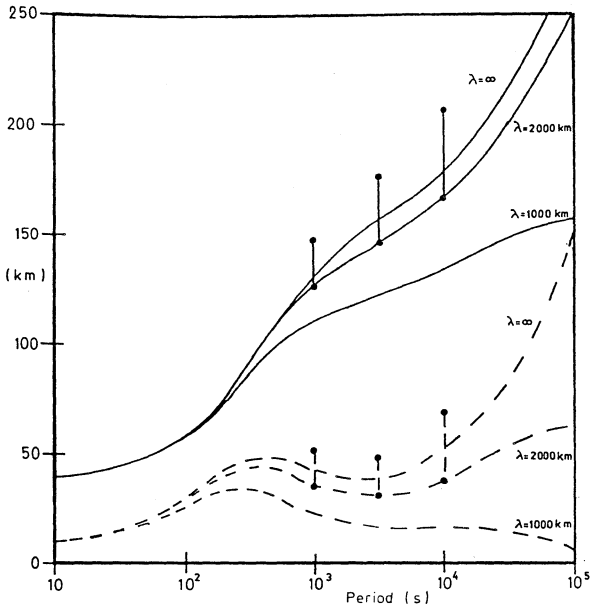

Fig. 13. Source effect on the parameters g (——) and h (— — —) for wavelengths of ∞, 2,000 km and 1,000 km. Also shown are the bounds of the parameters derived for a Gaussian electrojet source of half-width 500 km. The lower points correspond to measurements directly underneath the electrojet maximum, whilst the upper ones are for a position ±700 km from this maximum

"effective width" through averaging induction effects over a larger volume of the Earth during its lateral movement. If a Gaussian electrojet of half-width 500 km (as in the previous discussion) moves with a velocity of $500\,\mathrm{m\,s^{-1}}$, then $C(\omega,k)\sim C(\omega,0)$ for periods up to 5 h (2×10^4 s).

8. Conclusions

That magnetometer array studies are able not only to map the conductivity anomalies but also to determine the conductivity-depth distribution, where valid, has been known for a decade (Schmucker 1970). However, apart from three other studies, two of which derived the spatial gradient from Fourier maps (Kuckes 1973a; Lilley and Sloane 1976) and the third restricted to long periods (Woods and Lilley, 1979), the technique has not been much employed.

In this paper, the spatial gradient was determined by least-squares methods and the inductive response function by statistical frequency analysis techniques. The derived function was shown to be causal by two methods, *i*) the impulse response function $\bar{c}(\tau)$ did not react before receiving any input, and *ii*) the Hilbert Transform of the real part of $\bar{C}(\bar{\omega})$ closely resembles the imaginary part of $-\bar{C}((\bar{\omega})$. It was also shown to pass 7 of Weidelt's (1972) 9 inequality constraints imposed on it, and to be fully consistent in the time domain.

Because of the rather special property of the inductive response function, $C(\omega,k)$, that it is a function of k^2 and not of k, representation of the observed fields in terms of second-order polynomials results in a determination of $C(\omega,0)$, i.e., the uniform field response. Hence, this permits the data to be interpreted without regard to source-field configuration. A very preliminary conductivity-depth profile that explains the major details of the derived response function consists of three layers with the parameters ; $\rho_1=10^4\,\Omega$m; $\rho_2=125\,\Omega$m; $\rho_3=3.5\,\Omega$m; $d_1=30$ km; $d_2=140$ km. Using this model as a base, the effects of source contribution were shown to be important only for stationary sources of very small wavelength ($\lambda<1{,}000$ km) and at a point directly underneath the source maximum. Although the parameter k, wavenumber ($k=2\pi/\lambda$), is independent of the model parameters (Edwards et al. 1980), its effect closely resembles that of moving the conductive basement nearer to the surface. Hence it could be expected that other induction studies in the region, whose derived responses are affected by source-structure, would indicate a less deep highly conducting basement. Where magnetic variations exhibit a wavenumber which is a frequency constant, i.e., $k\neq fn(\omega)$, the derived conductivity profile from such studies may be transformed, by the algorithm given in Weidelt (1972), to yield the true conductivity-depth profile.

Acknowledgements. The author wishes to thank all those acknowledged in the paper by Küppers et al. (1979), and in addition J. Untiedt for continual support and guidance, F. Küppers for many reasons, and W. Baumjohann for discussion concerning source structure. The author is also very grateful to P. Weidelt for detailing the conditions placed on the inductive impulse response function, $c(t)$, as described in Sect. 2.3. All three referees are thanked for their constructive comments on an earlier version of this manuscript.

This work was supported in full by grants from the Deutsche Forschungsgemeinschaft, which are gratefully acknowledged.

References

Baumjohann, W., Greenwald, R.A., Küppers, F.: Joint magnetometer array and radar backscatter observations of auroral currents in northern Scandinavia. J. Geophys. **44**, 373–383, 1978

Baumjohann, W., Untiedt, J., Greenwald, R.A.: Joint two-dimensional observations of ground magnetic and ionospheric electric fields associated with auroral zone currents. 1. Three-dimensional current flows associated with a substorm-intensified eastward electrojet. J. Geophys. Res. **85**, 1963–1978, 1980

Bendat, J.S., Piersol, A.G.: Random data: analysis and measurement procedures. New York: Wiley-Interscience 1971

Berdichevsky, M.N., Fainberg, E.B., Rotanova, N.M., Smirnov, J.B., Vanyan, L.L.: Deep electromagnetic investigations. Ann. Géophys. **32**, 143–155, 1976

Cagniard, I.: Basic theory of the magnetotelluric method of geophysical prospecting. Geophysics **18**, 605–635, 1953

Champeney, D.C.: Fourier transforms and their physical application. London: Academic Press 1973

Čižek, V.: Discrete Hilbert Transform. IEEE Trans. Audio Electroacoust. **AU-18**, 340–343, 1970

Edwards, R.N., Bailey, R.C., Garland, G.D.: Crustal and upper mantle electrical conductivity studies with natural and artificial sources. Geophysics, submitted 1980

Ferris, C.D.: Linear network theory. Columbus, Ohio: Charles E. Merrill Books Inc. 1962

Fischer, G., Schnegg, P.-A.: The dispersion relations of the magnetotelluric response and their incidence on the inversion problem. Geophys. J.R. Astron. Soc. in press. 1980

Frazer, M.C.: Geomagnetic sounding with arrays of magnetometers. Rev. Geophys. Space Phys. **12**, 401–420, 1974

Golub, G.: Numerical methods for solving linear least-squares problems. Numerische Math. **7**, 206–216, 1965

Gough, D.I.: The interpretation of magnetometer array studies. Geophys. J.R. Astron. Soc. **35**, 85–98, 1973a

Gough, D.I.: The geophysical significance of geomagnetic variation anomalies. Phys. Earth Planet. Inter **7**, 379–388, 1973b

Gough, D.I., Reitzel, J.S.: A portable three component magnetic variometer. J. Geomagn. Geoelectr. **19**, 203–215, 1967

Hermance, J.F.: Electromagnetic induction in the Earth by moving ionospheric current systems. Geophys. J.R. Astron. Soc. **55**, 557–576, 1978

Hibbs, R.D., Jones, F.W.: The calculation of the electromagnetic fields of a sheet current source with arbitrary spatial intensity distribution over a layered half-space-I. The general method and results. Geophys. J.R. Astron. Soc. **46**, 433–452, 1976a

Hibbs, R.D., Jones, F.W.: The calculation of the electromagnetic fields of a sheet current source with arbitrary spatial intensity distribution over a layered half space – II. The computer program and its application. Geophys. J.R. Astron. Soc. **46**, 453–465, 1976b

Hildebrand, F.B.: Introduction to numerical analysis. New York: McGraw-Hill 1956

Jones, A.G.: Geomagnetic induction studies in southern Scotland. Ph.D. Thesis, University of Edinburgh 1977

Jones, A.G.: New coherence functions useful for determining the signal to random noise ratio in multivariate studies. IEEE Trans. Acoust., Speech, Signal Processing, submitted 1979

Jones, A.G.: On the reduction of bias in response function estimation for hand-digitised data. Geophys. J.R. Astron. Soc. submitted 1980

Jones, A.G., Hutton, R.: A multi-station magnetotelluric study in southern Scotland – II. Monte-Carlo inversion of the data and its geophysical and tectonic implications. Geophys. J.R. Astron. Soc. **56**, 351–368, 1979

Jones, A.G., Olafsdottir, B.: Geomagnetic induction studies in northern Scandinavia. Geophys. J.R. Astron. Soc. **57**, 265, 1979

Kanasewich, E.R.: Time sequence analysis in geophysics. Edmonton, Canada: University of Alberta Press 1973

Kuckes, A.F.: Relations between electrical conductivity of a mantle and fluctuating magnetic fields. Geophys. J.R. Astron. Soc. **32**, 119–131, 1973a

Kuckes, A.F.: Correspondence between the magnetotelluric and field penetration depth analysis for measuring electrical conductivity. Geophys. J.R. Astron. Soc. **32**, 381–385, 1973b

Küppers, F., Untiedt, J., Baumjohann, W., Lange, K., Jones, A.G.: A two-dimensional magnetometer array for ground-based observations of auroral zone electric currents during the International Magnetospheric Study. J. Geophys. **46**, 429–450, 1979

Lilley, F.E.M.: Magnetometer array studies: A review of the interpretation of observed fields. Phys. Earth Planet. Inter. **10**, 231–240, 1975

Lilley, F.E.M., Sloane, M.N.: On estimating electrical conductivity using gradient data from magnetometer arrays. J. Geomagn. Geoelectr. **28**, 321–328, 1976

Mersmann, U., Baumjohann, W., Küppers, F., Lange, K.: Analysis of an eastward electrojet by means of upward continuation of ground-based magnetometer data. J. Geophys. **45**, 281–298, 1979

Price, A.T.: The theory of magnetotelluric fields when the source field is considered. J. Geophys. Res. **67**, 1907–1918, 1962

Porath, H., Dziewonski, A.: Crustal resistivity anomalies from geomagnetic deep sounding studies. Rev. Geophys. Space Phys. **9**, 891–915, 1971

Schmucker, U.: Anomalies of Geomagnetic Variations in the Southwestern United States. Bull. Scripps Inst. Oceanogr., Univ. Calif. Press **13**, 1970

Schmucker, U., Weidelt, P.: Electromagnetic Induction in the Earth. Lect. Notes, Aarhus University, 1975

Solodovnikov, V.V.: Introduction to the statistical dynamics of automatic control systems. Chapter 1. (Translation edited by J.B. Thomas and L.A. Zadeh, Dover Publications Inc., New York, 1960), 1952

Srivastava, S.P.: Method of interpretation of magneto-telluric data when source field is considered. J. Geophys. Res. 70, 945–954, 1965

Untiedt, J., Pellinen, R., Küppers, F., Opgenoorth, H.J., Pelster, W.D., Baumjohann, W., Ranta, H., Kangas, J., Czechowsky, P., Heikkila, W.J.: Observations of the initial development of an auroral and magnetic substorm at magnetic midnight. J. Geophys. **45**, 41–65, 1978

Weidelt, P.: The inverse problem of geomagnetic induction. J. Geophys. **38**, 257–289, 1972

Weidelt, P.: Entwicklung und Erdprobung eines Verfahrens zur Inversion zweidimensionaler Leitfähigkeitsstrukturen in E-Polarisation. Habilitationsschrift Math.-Naturwiss. Fak. Univ. Göttingen, 1978

Westerlund, S.: Magnetotelluric experiments in the range 0.01 Hz to 10 kHz. KGO Report No. 72:10, Kiruna Geophysical Observatory, 1972

Woods, D.V., Lilley, F.E.M.: Geomagnetic induction in central Australia. J. Geomagn. Geoelectr. **31**, 449–458, 1979

Received April 11, 1980; Revised Version May 12, 1980
Accepted May 23, 1980